

Ordered Olivine-Type Lithium–Cobalt and Lithium–Nickel Phosphates Prepared by a New Precursor Method

Violeta Koleva,*^[a] Ekaterina Zhecheva,^[a] and Radostina Stoyanova^[a]

Keywords: Lithium / Cobalt / Nickel / Organic-inorganic hybrid composites / X-ray diffraction

Single phases of olivine-type LiCoPO_4 and LiNiPO_4 were synthesized by thermal treatment of homogeneous lithium–metal–phosphate–formate precursors obtained by freeze drying of aqueous solutions of the corresponding metal formates and LiH_2PO_4 . The structure, thermal behavior, and morphology of the precursors were studied by IR spectroscopy, DTA, and SEM. Cobalt and nickel phosphate–formate precursors have a composition $\text{LiMH}_x(\text{PO}_4)(\text{HCOO})_x\cdot y\text{H}_2\text{O}$, where the formate and phosphate groups are mainly deprotonated. For the Co precursor the formate and phosphates ions are randomly coordinated to both Co and Li cations, whereas for the Ni precursor there is a preferential coordina-

tion of the formate and phosphate ions around the Ni^{2+} and Li^+ ion, respectively. Thermal treatment of the precursors yields single phases of olivine-type LiCoPO_4 at 450 °C and LiNiPO_4 at 700 °C. Structural analysis evidences that both LiCoPO_4 and LiNiPO_4 have an ordered olivine-type structure without any Li to M disorder between the metal positions and lithium deficiency. The effect of the freeze-dried solution concentration and annealing temperature on the structure, crystallite size, and morphology of LiCoPO_4 and LiNiPO_4 has been discussed. The morphology of the cobalt and nickel phospho-olivines comprises isometric particles with mean sizes of 190 and 380 nm, respectively.

Introduction

Lithium–transition metal orthophosphates with olivine-type structure (LiMPO_4 , M = Fe, Mn, Co, and Ni) are the most intensive studied compounds as cathode materials for lithium-ion batteries in the last years. This is a consequence of their high cycling stability, tolerance to overcharge, and safety.^[1,2] The best electrochemical performance is achieved with the iron analogue LiFePO_4 . The electrochemical reaction takes place by reversible lithium intercalation in the olivine structure concomitantly with the oxidation/reduction of Fe^{2+} to Fe^{3+} , the operating voltage being 3.4 V. By simple replacement of iron by manganese, cobalt, and nickel, a higher operating voltage and energy density of the phospho-olivines can be achieved, which is beneficial for their electric vehicle applications. Cobalt and nickel phospho-olivines exhibit higher operating voltages (4.8 and 5.1 V vs. Li^+/Li) and energy densities (227.4 and 250.2 Wh/kg).^[3–5] The main drawback of the phospho-olivines is their low electronic and ionic conductivity. To overcome this drawback, specific synthesis methods have to be developed that aim to minimize the dimensions of the particles and/or to cover them with conductive substances. In this topic, a lot of work is carried out on the preparation of LiFePO_4 and LiMnPO_4 , whereas the reports on the preparation of LiCoPO_4 and LiNiPO_4 are limited.

LiCoPO_4 has been prepared by using solid-state reactions^[3,6,7] and soft chemistry routes.^[8–13] A common feature of all synthetic methods is the relatively high temperature where LiCoPO_4 is formed (600–800 °C and prolonged heating). Concerning LiNiPO_4 , solid-state reactions,^[4,14] sol-gel,^[9] and coprecipitation^[15] methods are used, but in all cases the synthesis temperature exceeds 775 °C.

Recently, we developed a phosphate–formate precursor method for the preparation of nano-sized olivine-type LiFePO_4 .^[16] The method is based on the formation of homogeneous lithium–iron–phosphate–formate precursors by freeze drying aqueous solutions containing lithium, iron(II), phosphate, and formate ions. Thermal treatment of the lithium–iron–phosphate–formate precursors at temperatures above 300 °C yields nanometric LiFePO_4 (particle sizes between 60 and 100 nm) containing up to 2 mass% carbon. The advantage of this method is related to the ability to control the morphology of lithium–iron–phosphate–formate precursors by a simple variation of the concentration of the freeze-dried solutions. This, on its turn, has an impact on the carbon content, particles size distribution, and electrochemical properties of target LiFePO_4 .^[17] The aptitude of the phosphate–formate precursor method to design simultaneously precursors and the target product has also been demonstrated with the preparation of nanocrystalline manganese phospho-olivine LiMnPO_4 .^[18] By this method a new structural modification of LiNiPO_4 (with Na_2CrO_4 -type structure) has been prepared.^[19]

In this paper we examine the applicability of the phosphate–formate precursor method for the preparation of co-

[a] Institute of General and Inorganic Chemistry, Bulgarian Academy of Sciences, Acad. G. Bonchev St, bl. 11, 1113 Sofia, Bulgaria
Fax: +359-2-8705024
E-mail: vkoleva@svr.igic.bas.bg

balt and nickel phospho-olivines, LiCoPO_4 and LiNiPO_4 . The precursors and target LiCoPO_4 and LiNiPO_4 compositions were characterized by XRD, IR spectroscopy, DTA, and SEM. The mechanism of cobalt and nickel phospho-olivines formation is discussed on the basis of iron and manganese analogues.

Results and Discussion

Composition and Structure of the Li–M–Phosphate–Formate Precursors (M = Co and Ni)

Freeze drying of the solution containing Li^+ , Co^{2+} or Ni^{2+} , PO_4^{3-} and HCOO^- in the ratio 1:1:1:2 yields amorphous powders with compositions as follows: pink $\text{LiCoH}_x(\text{PO}_4)_y(\text{HCOO})_z \cdot y\text{H}_2\text{O}$ ($x \approx 1$ and $y \approx 1.5$) and pale green $\text{LiNiH}_x(\text{PO}_4)_y(\text{HCOO})_z \cdot y\text{H}_2\text{O}$ ($x \approx 1.2$; $2.5 < y < 2.7$). The precursor compositions do not depend on the concentration of freeze-dried solutions. These results evidence for partial formic acid sublimation during the freeze-drying process: 1 and 0.8 mol of HCOOH are sublimated in the case of Co and Ni precursors, respectively. The same results were established for the iron and manganese phosphate–formate precursors,^[16,18] where only 1 mol of HCOOH is sublimated.

To examine the form and type of coordination of the anion groups in the freeze-dried compositions, IR spectroscopy was undertaken. Figures 1 and 2 give the IR spectra of Co and Ni freeze-dried precursors. For the sake of comparison, the IR spectra of $\text{M}(\text{HCOO})_2 \cdot 2\text{H}_2\text{O}$ and $\text{M}(\text{H}_2\text{PO}_4)_2 \cdot 2\text{H}_2\text{O}$ (M = Co, Ni) are also presented. The dihydrogen phosphates were synthesized as described elsewhere.^[20]

Three groups of IR bands due to the vibrations of formates, phosphates, and OH groups are resolved in the spectra of the precursors. It is noticeable that the concentration of the freeze-dried solution does not affect the IR profiles. The analysis of the IR spectra of both Co and Ni precursors reveals the presence of the characteristic IR vibrations due to deprotonated formate ions:^[21] $\nu_{\text{as}}(\text{COO})$ at 1607–1584 cm^{-1} ; $\delta(\text{CH})$ in the range 1399–1393 cm^{-1} ; $\nu_{\text{s}}(\text{COO})$ in the range 1378–1355 cm^{-1} , and $\delta_{\text{s}}(\text{OCO})$ in the range 795–774 cm^{-1} . All these characteristic vibrations are clearly seen in the IR spectra of the initial Co and Ni formate salts, $\text{M}(\text{HCOO})_2 \cdot 2\text{H}_2\text{O}$ (M = Co, Ni). Close inspection of Figure 2 shows that the wavenumbers of $\delta(\text{CH})$ and $\nu_{\text{s}}(\text{COO})$ vibrations are the same for the Ni precursor and for pure $\text{Ni}(\text{HCOO})_2 \cdot 2\text{H}_2\text{O}$. Therefore, one can suggest that for the Ni precursor the formate ions are predominantly coordinated to the Ni^{2+} ions. Contrary to Ni, it appears that for the Co precursors the formate ions are coordinated simultaneously to both Co^{2+} and Li^+ .

The vibrations associated with the deprotonated phosphate ion (PO_4^{3-}) are also well seen in the IR spectra of the Co(Ni) precursors (Figures 1 and 2). The two bands in the 1080–1008 cm^{-1} range for the Co precursors and the band at 1060 cm^{-1} for the Ni precursors are due to the asymmetric ν_3 stretching vibrations of the PO_4^{3-} ions. The doublets

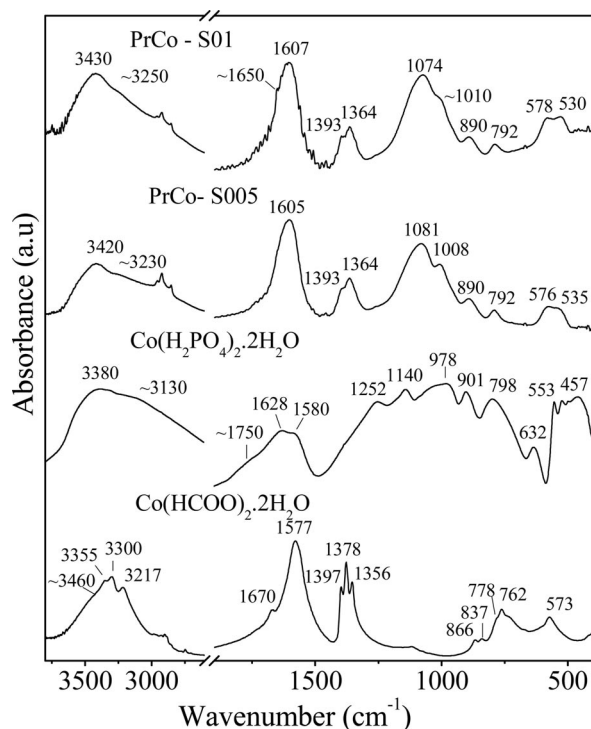


Figure 1. IR spectra of $\text{Co}(\text{HCOO})_2 \cdot 2\text{H}_2\text{O}$, $\text{Co}(\text{H}_2\text{PO}_4)_2 \cdot 2\text{H}_2\text{O}$, and lithium–cobalt–phosphate–formate precursors.

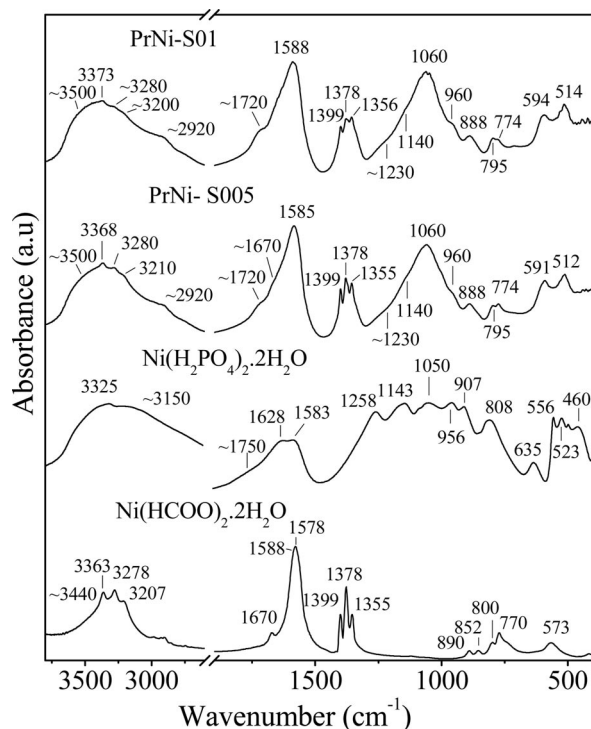


Figure 2. IR spectra of $\text{Ni}(\text{HCOO})_2 \cdot 2\text{H}_2\text{O}$, $\text{Ni}(\text{H}_2\text{PO}_4)_2 \cdot 2\text{H}_2\text{O}$, and lithium–nickel–phosphate–formate precursors.

at 578/530 and 594/514 cm^{-1} for the Co and Ni precursors, respectively, are associated with the asymmetric ν_4 bending PO_4^{3-} vibrations.^[22] It is worth mentioning that the positions of the ν_3 and ν_4 vibrations for the PO_4^{3-} ions in the

Ni precursors are close to those observed for Li_3PO_4 at 1040 and 592 cm^{-1} .^[23] Hence, it appears that the phosphate ions in the Ni precursors are preferentially coordinated around the Li^+ ions.

In addition, the Ni precursor exhibits three low intensive bands at 960, ca. 1230, and 1720 cm^{-1} (Figure 2). These bands can be attributed to the protonated forms of the coordinated anions – HCOOH and/or H_2PO_4^- or HPO_4^{2-} . To analyze this feature, the characteristic vibrations of protonated HCOOH and/or H_2PO_4^- or HPO_4^{2-} groups are taken into account: for HCOOH , the $\nu(\text{C}=\text{O})$, $\nu(\text{C}-\text{O})$, and $\gamma(\text{OH})$ vibrations are at 1700, 1260 and 975 cm^{-1} ,^[24] whereas for the protonated phosphate ions (H_2PO_4^- or HPO_4^{2-}) the out-of-plane $\delta(\text{OH})$ and in-plane $\gamma(\text{OH})$ bending POH vibrations are at 1230–1260 and $800\text{--}900\text{ cm}^{-1}$.^[25,26] The comparison shows that the three additional bands at 1720, 1230, and 960 cm^{-1} are due to HCOOH rather than to protonated phosphate ions. The presence of small amount of protonated HCOOH is in accordance with the chemical composition of the Ni precursor, where the amount of formate species is higher than 1 mol.

In the range of the stretching OH vibrations, two bands at 3430 and ca. 3250 cm^{-1} are observed for the Co precursors, whereas there are four bands between 3500 and 3200 cm^{-1} for the Ni precursors. The bending water vibration is seen at $1650\text{--}1670\text{ cm}^{-1}$. For the Ni precursors, the positions of the four OH bands are close to that in initial $\text{Ni}(\text{HCOO})_2 \cdot 2\text{H}_2\text{O}$ (Figure 2). For the sake of comparison, for $\text{LiHCOO} \cdot \text{H}_2\text{O}$ these bands are at 3398 and 3109 cm^{-1} .^[27] This comparison shows that the water molecules are mainly coordinated to the nickel ions in the Ni precursors. The difference in the positions of OH vibrations for the cobalt precursors and $\text{Co}(\text{HCOO})_2 \cdot 2\text{H}_2\text{O}$ (Figure 1) and $\text{LiHCOO} \cdot \text{H}_2\text{O}$ ^[27] reveals that water molecules are coordinated to both cobalt and lithium ions in the cobalt precursors.

Summarizing, two features concerning the form and the type of coordination of the anionic groups and water molecules in the Co and Ni precursors can be outlined. First, in both types of precursors the formate and phosphate groups are mainly deprotonated. Second, there is a difference in respect to the type of coordination of the anionic groups and water molecules. Thus, in the Co precursors the formate and phosphate ions and the water molecules are coordinated to both types of cations without any preference. A similar feature was established for the Fe and Mn precursors obtained by the same freeze-drying method.^[16,18] Contrary, in the case of Ni precursors the formate ions and the water molecules prefer to coordinate the Ni^{2+} ions, whereas the phosphate ions coordinate the Li^+ ions. This is a specific feature of the Ni precursors obtained by freeze-drying of mixed phosphate–formate solutions.

The Ni and Co precursors exhibit not only a different structure, but also a different morphology. Figure 3 gives the SEM images of both precursors. Whereas the morphology of the Co precursors consists of flake-like aggregates, the Ni precursors display “cabbage”-like aggregates.

By increasing the concentration of the freeze-dried solutions, there is a slight tendency for increasing the aggregate dimensions of the Ni precursors. It is worth noting that a flake-like morphology was established for the iron and

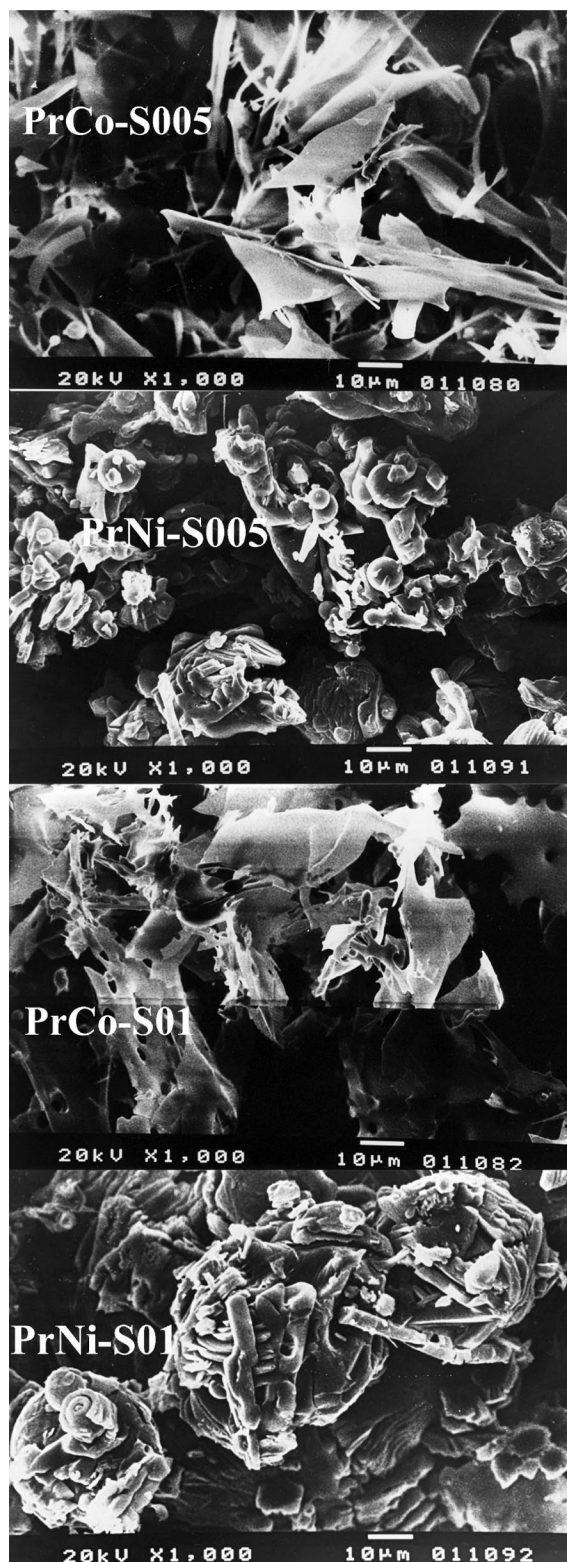


Figure 3. SEM images of LiCo- and LiNi-phosphate-formates precursors.

manganese phosphate–formate precursors. This result demonstrates once again the difference in the formation of the Ni precursors by freeze drying of solutions. The different structure and morphology of the Ni precursors as compared to that of Co, Mn, and Fe precursors can be related with the complex equilibria in the metal–phosphate–formate solutions.

The thermal properties of the Li–M–phosphate–formate (M = Co, Ni) precursors were followed by differential thermal analysis (Figures 4 and 5). For both compositions, endothermic peaks between 50 and 200 °C accompanied with a mass loss are clearly observed. These peaks can be related with dehydration processes, as was observed for the thermal decomposition of $M(\text{HCOO})_2 \cdot 2\text{H}_2\text{O}$ (M = Co, Ni)^[28,29] and LiHCOO .^[30] According to the TG curves they correspond to the release of 1.5 and 2.7 mol H_2O molecules from the Co and Ni precursor, respectively. Above 200 °C, the decomposition of the formate species occurs, which is registered on the DTA curves with several endo- and exothermic effects. In addition, the decomposition process is more complex and finishes at higher temperatures for the Ni precursor: the total mass loss for the Ni precursor up to 550 °C is 38.8%, whereas for the Co precursor the total mass loss is 31.1% up to 400 °C. This is a result of the appearance of more than one mol of formate species in the Ni precursor.

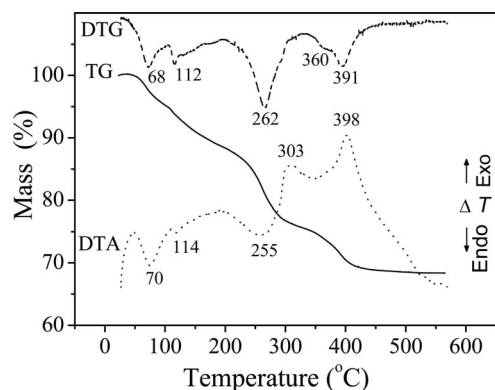


Figure 4. TG, DTA, and DTG curves for PrCo-S005.

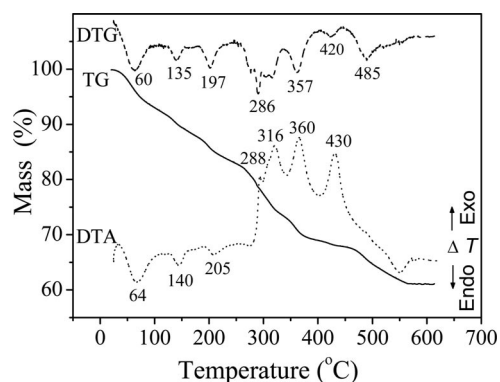


Figure 5. TG, DTA, and DTG curves for PrNi-S005.

Structural and Morphological Characterization of LiMPO_4 (M = Co, Ni)

LiCoPO_4

The XRD patterns of PrCo-S005 annealed between 350 and 600 °C is shown on Figure 6. The XRD analysis shows that olivine-type LiCoPO_4 is already formed at 350 °C. In addition, the partially decomposed precursor at 350 °C comprises also impurity phases including CoO , Li_3PO_4 , Co_3O_4 , $\text{Co}_2\text{P}_2\text{O}_7$, and an unknown phase with a strong diffraction peak at $2\theta = 22.14^\circ$. The phase composition is the same for the samples obtained from diluted and concentrated freeze-dried solutions. Further annealing of the samples leads to a decrease in the amount of the impurity phases, culminating at 450 °C in the formation of a single phase of well-crystallized LiCoPO_4 . To the best of our knowledge this is the lowest synthesis temperature that was reported for pure olivine-type LiCoPO_4 . The data obtained reveal that the formation of LiCoPO_4 from the phosphate–formate precursors takes place through interaction between Li_3PO_4 , $\text{Co}_2\text{P}_2\text{O}_7$, and cobalt oxides (CoO and/or Co_3O_4). The same mechanism of phospho-olivine formation was established also for LiMnPO_4 .^[18] Contrary to Co and Mn phospho-olivines, a single LiFePO_4 phase is formed directly after the release of the formic acid (i.e., at 350 °C), which is

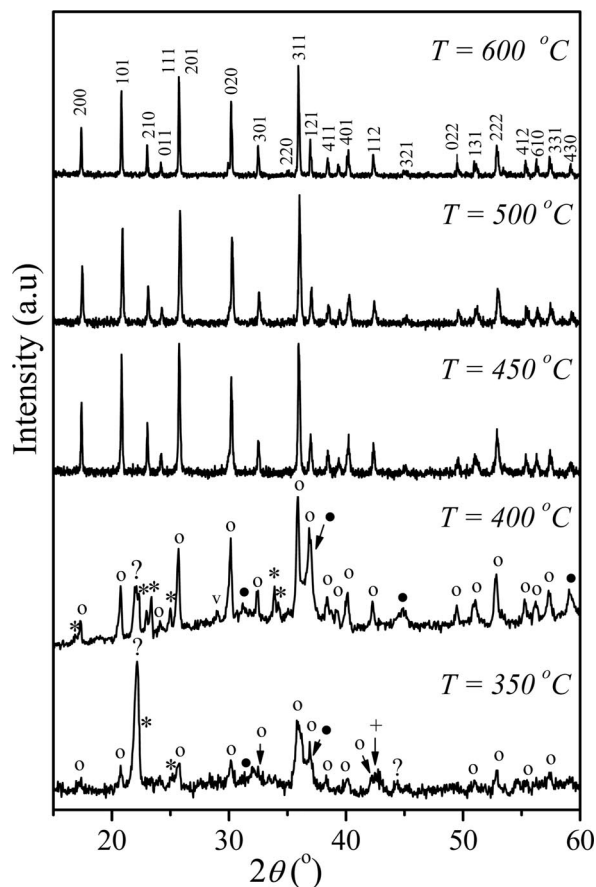


Figure 6. XRD patterns of PrCo-S005 annealed between 350 and 600 °C. Symbols: olivine-type LiCoPO_4 (O), Li_3PO_4 (*); CoO (+), Co_3O_4 (●), $\text{Co}_2\text{P}_2\text{O}_7$ (v), unknown phase (?).

accompanied with carbon deposition (up to 2.5 mass%).^[16] Contrary, no carbon was detected for the LiMnPO₄ and LiCoPO₄ samples. This demonstrates the different mechanism of formation of LiCo/MnPO₄ and LiFePO₄ from phosphate–formate precursors.

The XRD patterns of LiCoPO₄ obtained between 450 and 600 °C are satisfactory fitted by Rietveld analysis on the basis of the model of an ideal olivine structure, *SG Pnma* (Figure 7) and the structural parameters are given in Table 1. The lattice parameters and unit cell volumes seems to be insensitive towards both the annealing temperature and the concentration of the freeze-dried solutions. For the fitting procedure a possible Li/Co disorder between the *4a* and *4c* sites was also tried. However, after the refinement the occupancy factors of Li at *4a* and Co at *4c* tend to 1 (within the experimental error). For LiCoPO₄ annealed at 450 °C, the fitting procedure gives $R_b = 3.86$ with Li/Co disorder of 0.0035 ± 0.0015 vs. $R_b = 4.00$ without disorder; for LiCoPO₄ annealed at 500 °C – $R_b = 3.48$ with Li/Co disorder of 0.0018 ± 0.0014 vs. $R_b = 3.56$ without disorder; for LiCoPO₄ annealed at 600 °C – $R_b = 5.29$ with Li/Co disorder of 0.0044 ± 0.0014 vs. $R_b = 5.30$ without disorder. On the basis of the Rietveld refinement of neutron and X-ray powder diffraction, Ehrenberg et al.^[31] reported a Li deficiency at *4a* site (92% occupancy) for LiCoPO₄ obtained by the citric-assisted Pechini method at 600 °C. We have also tested a Li deficiency at *4a*, but the refinement results rejected this possibility: for LiCoPO₄ annealed at 450 °C R_b is 4.06 for *4a* site occupancy of 0.980 ± 0.020 ; for LiCoPO₄ annealed at 500 °C R_b is 3.53 for *4a* site occupancy of 1.010 ± 0.010 ; for LiCoPO₄ annealed at 600 °C R_b is 5.39 for *4a* site occupancy of 1.020 ± 0.020 . This means that LiCoPO₄ without any Li/Co disorder and Li deficiency is formed from phosphate–formate precursors between 450 and 600 °C. For comparison, LiMnPO₄ samples prepared by the same method at 500–600 °C are characterized by an ordered olivine-type structure, whereas at a lower temperature (450 °C) a small Li/Mn disorder of 2.6% between *4a* and *4c* sites was found.^[18]

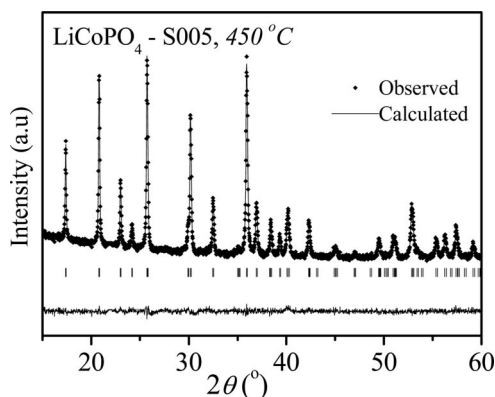


Figure 7. Rietveld refinement of the XRD pattern of PrCo-S005 annealed at 450 °C.

The results from XRD analysis are confirmed by the IR spectroscopic data (Figure 8). The decomposition of the

Table 1. Structural parameters of LiMPO₄ (M = Co and Ni) determined by Rietveld analysis.

Atom	Site	<i>x</i>	<i>y</i>	<i>z</i>	<i>B</i> (Å ²)	SOF ^[a]
LiCoPO ₄ -S005, 450 °C						
$a = 10.2026(3) \text{ \AA}$, $b = 5.9212(1) \text{ \AA}$, $c = 4.6995(1) \text{ \AA}$						
$V = 283.907(16) \text{ \AA}^3$						
$R_{wp} = 11.7$, $R_b = 4.00$, $R_f = 3.57$						
Li	<i>4a</i>	0	0	0	1.1	1.0
Co	<i>4c</i>	0.2788(1)	1/4	0.9791(5)	0.9	1.0
P	<i>4c</i>	0.0958(3)	1/4	0.4200(7)	1.0	1.0
O1	<i>4c</i>	0.0955(7)	1/4	0.743(1)	0.9	1.0
O2	<i>4c</i>	0.4547(9)	1/4	0.205(1)	0.9	1.0
O3	<i>8d</i>	0.1654(8)	0.0458(7)	0.2853(8)	0.9	2.0
LiCoPO ₄ -S005, 500 °C						
$a = 10.2045(2) \text{ \AA}$, $b = 5.9213(1) \text{ \AA}$, $c = 4.7002(1) \text{ \AA}$						
$V = 284.012(14) \text{ \AA}^3$						
$R_{wp} = 10.90$, $R_b = 3.56$, $R_f = 3.76$						
Li	<i>4a</i>	0	0	0	1.2	1.0
Co	<i>4c</i>	0.2787(1)	1/4	0.9789(4)	1.3	1.0
P	<i>4c</i>	0.0951(3)	1/4	0.4186(6)	1.1	1.0
O1	<i>4c</i>	0.0958(6)	1/4	0.745(1)	0.9	1.0
O2	<i>4c</i>	0.4561(8)	1/4	0.2060(9)	0.9	1.0
O3	<i>8d</i>	0.1670(5)	0.0456(6)	0.2848(7)	0.9	2.0
LiCoPO ₄ -S005, 600 °C						
$a = 10.2057(1) \text{ \AA}$, $b = 5.9228(1) \text{ \AA}$, $c = 4.7009(1) \text{ \AA}$						
$V = 284.161(7) \text{ \AA}^3$						
$R_{wp} = 10.30$, $R_b = 5.29$, $R_f = 6.84$						
Li	<i>4a</i>	0	0	0	1.1	1.0
Co	<i>4c</i>	0.2787(1)	1/4	0.9785(4)	0.9	1.0
P	<i>4c</i>	0.0955(2)	1/4	0.4204(6)	1.0	1.0
O1	<i>4c</i>	0.0978(5)	1/4	0.744(1)	0.9	1.0
O2	<i>4c</i>	0.4543(7)	1/4	0.2069(9)	0.9	1.0
O3	<i>8d</i>	0.1658(4)	0.0456(6)	0.2823(7)	0.9	2.0
LiNiPO ₄ -S005, 700 °C						
$a = 10.0384(1) \text{ \AA}$, $b = 5.85945(5) \text{ \AA}$, $c = 4.68020(5) \text{ \AA}$						
$V = 275.288(5) \text{ \AA}^3$						
$R_{wp} = 8.32$, $R_b = 3.37$, $R_f = 4.83$						
Li	<i>4a</i>	0	0	0	1.1	1.0
Ni	<i>4c</i>	0.2757(1)	1/4	0.9821(2)	1.2	1.0
P	<i>4c</i>	0.0952(2)	1/4	0.4199(4)	1.1	1.0
O1	<i>4c</i>	0.0996(3)	1/4	0.7450(7)	0.7	1.0
O2	<i>4c</i>	0.4503(4)	1/4	0.2019(6)	0.7	1.0
O3	<i>8d</i>	0.1647(3)	0.0447(4)	0.2760(4)	0.7	2.0

[a] The site occupation factors (SOF) are given as number of atoms per formula unit.

LiCo precursors is completed for a short heating time at 350 °C (3 h) after the release of formic acid. The IR spectrum does not display any IR bands due to the formate ions vibrations. There are only bands due to the stretching PO and bending OPO vibrations. By extending the heating time from 3 to 10 h, the characteristic PO₄³⁻ ion vibrations become more resolved. The LiCo samples annealed at 450 °C exhibit the typical IR spectrum for well crystalline olivine-type LiCoPO₄:^[32] $\nu_3(\text{PO}_4)$ modes in the region 1149–976 and $\nu_4(\text{PO}_4)$ modes in the region 646–550 cm⁻¹. The bands at 521 and 471 cm⁻¹ are suggested to originate mainly from Li⁺ translations.^[32] The bands positions are independent on the annealing temperature, which evidences the good thermal stability of the obtained LiCoPO₄ powders.

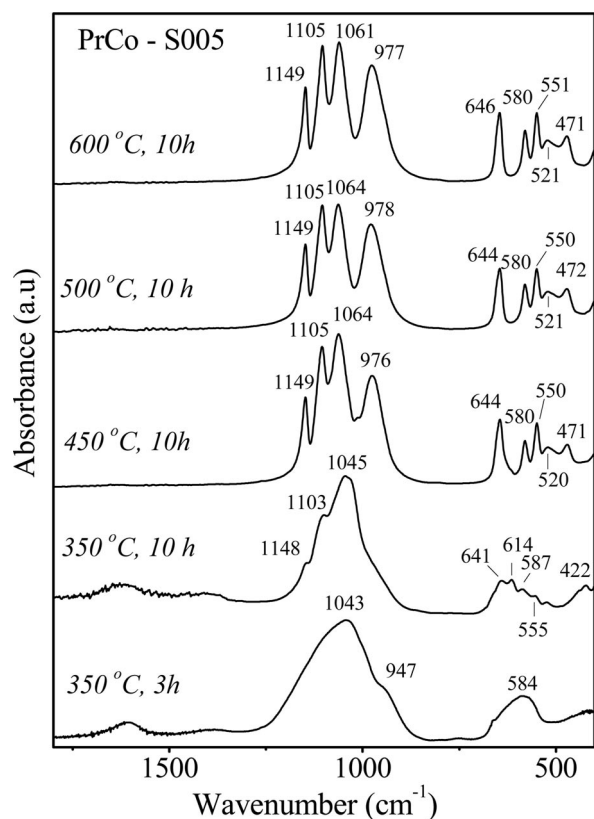


Figure 8. IR spectra of PrCo-S005 annealed between 350 and 600 °C.

The influence of the initial solution concentration and the annealing temperature on the LiCoPO_4 morphology is demonstrated by SEM analysis (Figure 9). The corresponding particles size distributions as determined from SEM analysis are also given (Figure 9, right). The morphology of LiCoPO_4 consists of isometric particles with close size distribution and does not depend on the solution concentration: the mean particles dimensions are around 185 ± 35 and 190 ± 30 nm for powders obtained at 500 °C from 0.05 and 0.10 M solutions, respectively (Figure 9A and B). By increasing the annealing temperature from 500 to 600 °C, there is a particle growth (around 230 ± 40 nm) and particle size distribution is slightly disturbed (Figure 9C). In addition, the crystallite sizes of LiCoPO_4 determined from the X-ray diffraction line broadening fall in the nanometric range (between 70 and 100 nm, Figure 10). On increasing the annealing temperature, the crystallite sizes tend to increase. Furthermore, the crystallite sizes slightly increase with the concentration of the freeze-dried solutions. It is worth mentioning that the crystallite sizes are slightly lower than the particle size dimensions determined from SEM analysis.

LiCoPO_4 obtained from phosphate–formate precursors is characterized with particles having small dimensions. In the literature, there are several reports on the formation of LiCoPO_4 with particle dimensions varying from 50 nm to 5 μm : for LiCoPO_4 obtained by solid-state reactions the particles were about 200–300 nm^[6] and 0.5–5 μm ,^[7] for

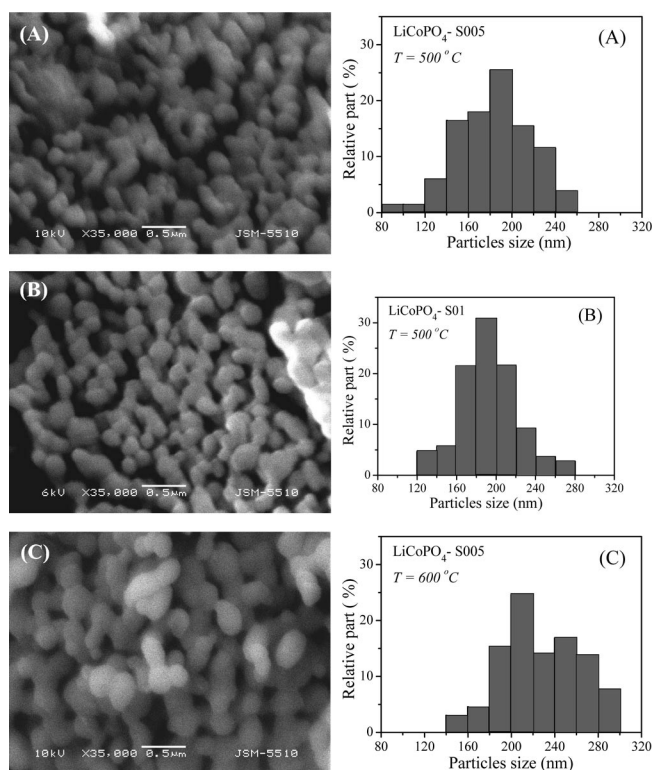


Figure 9. SEM images (left column) and corresponding particles size distributions (right column) of LiCoPO_4 .

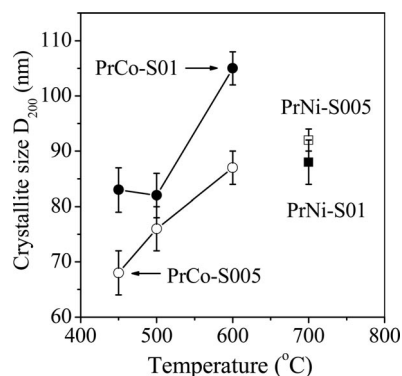


Figure 10. Dependence of the crystallite size D_{200} on the synthesis temperature for LiCoPO_4 and LiNiPO_4 prepared from two freeze-dried solutions. Symbols: LiCoPO_4 prepared from 0.05 M solution (\circ) and 0.10 M solution (\bullet), LiNiPO_4 prepared from 0.05 M solution (\square) and 0.10 M solution (\blacksquare).

LiCoPO_4 obtained by microwave heating the particles were about 400 nm² μm ,^[13] and for LiCoPO_4 prepared from citric acid assisted sol–gel method the particles were about 50 nm.^[9] The particles sizes of LiCoPO_4 were reduced to about of 100–150 nm by addition of conductive carbon during the synthesis^[6,13] or by subsequent high-energy ball milling.^[7] The comparison shows that the phosphate–formate precursor method allows preparing LiCoPO_4 with small particles, which will be favorable for its electrochemical performance.

Because the iron, manganese, and cobalt phosphate–formate precursors have a close structure and mor-

phology,^[16,18] it deserves to compare the particle dimensions and the crystallite sizes of the target LiMPO₄ olivines. The results show that the particle dimensions and crystallite sizes increase in the following order: LiFePO₄ < LiMnPO₄ < LiCoPO₄. The observed order can be related with the specific features of their formation: LiFePO₄ is directly formed after decomposition of the phosphate–formate precursor, whereas both LiMnPO₄ and LiCoPO₄ are a result of the solid-state reaction between the decomposition products. Further, the formation of LiCoPO₄ proceeds in air, whereas an argon atmosphere is needed for LiMnPO₄.

LiNiPO₄

The XRD patterns of PrNi-S005 annealed at temperatures between 400 and 750 °C for 10 h are depicted in Figure 11. Thermal treatment of the LiNi–formate–phosphate precursors at 400 °C yields a phase mixture of metal Ni, NiO, and lithium phosphates phases like Li₃PO₄ and Li₄P₂O₇. LiNiPO₄ is formed at a temperature higher than 400 °C through a solid-state reaction between nickel oxide and lithium phosphates. A characteristic feature is that the LiNiPO₄ composition at 500 °C represents a phase mixture between two structural modifications: olivine-type and Na₂CrO₄-type modifications (denoted also as β'-phase in^[33]). The mechanism of formation of the two forms of LiNiPO₄ from a LiNi–phosphate–formate precursor was discussed in our previous communication.^[19] The appearance of the metastable Na₂CrO₄-type modification of LiNiPO₄ at 500 °C is a specific feature of the phosphate–formate precursor method for the Ni analogue. This reveals, most probably, once again the different structure and morphology of the nickel–phosphate–formate precursor.

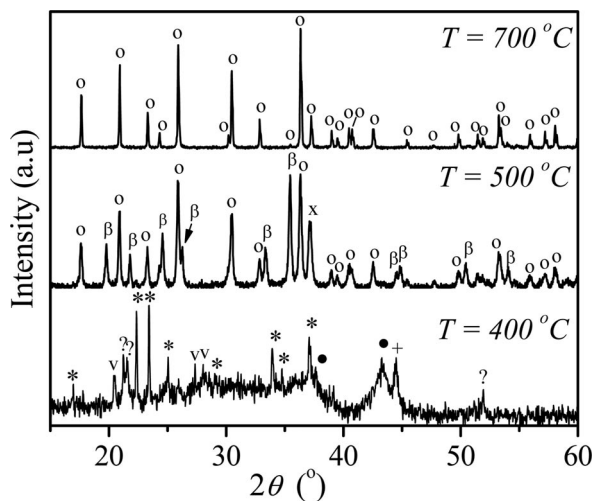


Figure 11. XRD patterns of PrNi-S005 annealed between 400 and 700 °C. Symbols: Li₃PO₄ (*), metal Ni (+), NiO (●), Li₄P₂O₇ (v), unknown phase (?), Na₂CrO₄-type LiNiPO₄ (β), olivine-type LiNiPO₄ (O), common peak (x).

The temperature-induced transformation of the metastable Na₂CrO₄-type to the olivine-type LiNiPO₄ is finished at 700 °C (Figure 11). Figure 12 and Table 1 give the results of the Rietveld refinement based on an ideal olivine-type

structure of the XRD pattern of LiNiPO₄ annealed at 700 °C. As in the case of LiCoPO₄, the structural analysis reveals the formation of an olivine-type LiNiPO₄ phase, *SG Pnma*, without any Li/Ni disorder (between *4a* and *4c* positions) and Li deficiency: $R_b = 3.18$ with Li/Ni disorder of 0.004 ± 0.002 vs. $R_b = 3.29$ for *4a* site occupancy of 1.020 ± 0.020 vs. $R_b = 3.37$ without Li/Ni disorder and Li deficiency. In addition, the unit cell parameters of LiNiPO₄ do not depend on the concentration of the freeze-dried solutions.

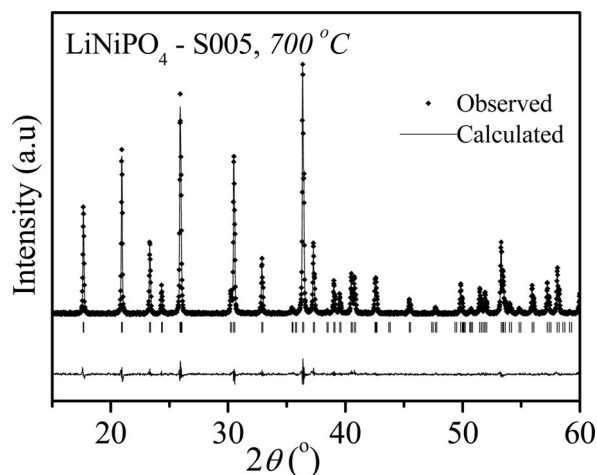


Figure 12. Rietveld refinement of the XRD pattern of PrNi-S005 annealed at 700 °C.

Figure 13 shows the IR spectra of the samples annealed between 400 and 700 °C. The IR spectrum at 400 °C is dominated by the absorption bands of phosphate groups in the regions of 1150–900 and 650–500 cm⁻¹. The weak bands around 1630, 1400, and 750 cm⁻¹ are related with residual formate species. In accordance with the XRD data, the IR

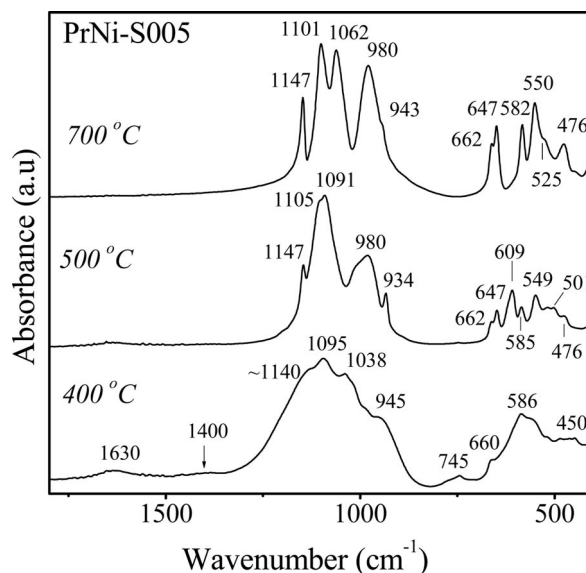


Figure 13. IR spectra of PrNi-S005 annealed between 400 and 700 °C.

spectrum of the sample annealed at 500 °C displays absorption bands due to the two LiNiPO₄ phases. The bands at 934, 609 and 501 cm⁻¹ (ν_1 , ν_4 , and ν_2 modes, respectively) are attributed to the Na₂CrO₄-type form only, whereas the residual bands originate from both forms. The IR spectrum of the sample at 700 °C fully coincides with that of pure olivine-type LiNiPO₄^[32] (Figure 13): $\nu_1(\text{PO}_4)$ vibration at 943 cm⁻¹, $\nu_3(\text{PO}_4)$ vibrations in the region 1147–980 cm⁻¹, $\nu_4(\text{PO}_4)$ vibration in the region 662–550 cm⁻¹, and Li⁺-translations in the range 525–476 cm⁻¹.

Figure 14 depicts the SEM image of the olivine-type LiNiPO₄ prepared by the phosphate–formate method at 700 °C. As in the case of LiCoPO₄, the morphology of LiNiPO₄ comprises isometric particles with a higher mean size of 380 ± 70 nm and a broader particle size distribution. The particle size derived from SEM is larger than the crystallite size derived from XRD (about 90 nm, Figure 10). This means that the SEM particles are not single crystals. It is worth mentioning that there are no data in the literature for morphological characterization of LiNiPO₄.

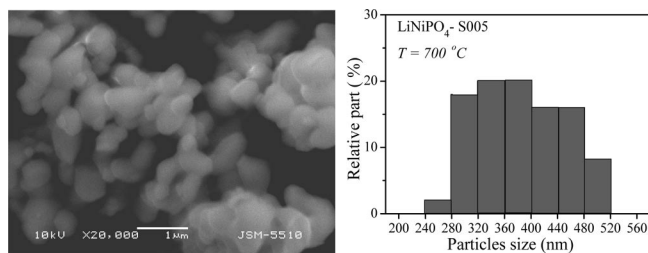


Figure 14. SEM image and particles size distribution of LiNiPO₄ annealed at 700 °C.

Conclusion

Homogeneous lithium–metal–phosphate–formate precursors with a composition LiMH_x(PO₄)(HCOO)_x·yH₂O (M = Co, Ni) were prepared by freeze drying of aqueous solutions of the corresponding metal formates and LiH₂PO₄. Cobalt and nickel precursors have different structure and morphology. Whereas in the Co precursors the formate and phosphates ions are randomly coordinated to both Co and Li cations, in the Ni precursors the formate ions are preferentially around Ni²⁺ and the phosphate ions are around Li⁺. The morphology of the Co precursors consists of flake-like aggregates, whereas the “cabbage”-like aggregates are formed for the Ni precursors. Nickel phosphate–formate precursors are decomposed at higher temperatures in comparison with the Co analogues. Thermal treatment of the precursors yields single olivine-type LiCoPO₄ at 450 °C and LiNiPO₄ at 700 °C with crystallite sizes of 65 and 90 nm, respectively. LiCoPO₄ and LiNiPO₄ phases display isometric particles with mean SEM particle dimensions of 185 and 380 nm, respectively. For both Co and Ni systems, the phosphate–formate precursor method yields olivine-type phase without any Li to M disorder (between 4a and 4c positions) and Li deficiency. A specific feature of LiNiPO₄ is that a phase mixture between olivine-

type and Na₂CrO₄-type structural modifications is formed at 500 °C. The Na₂CrO₄-type modification of LiNiPO₄ is transformed to olivine-type LiNiPO₄ at 700 °C.

Experimental Section

Preparation of Lithium–Cobalt–Phosphate–Formate and Lithium–Nickel–Phosphate–Formate Precursors: The starting reagents are M(HCOO)₂·2H₂O (M = Co, Ni) and LiH₂PO₄ (Aldrich). The metal formate dihydrates, M(HCOO)₂·2H₂O, were prepared by neutralization of dilute formic acid solutions with the corresponding carbonates at 60–70 °C. The solutions were then filtered and concentrated. The crystals M(HCOO)₂·2H₂O (M = Co, Ni) grew by cooling at room temperature. They are very stable upon storage, which ensures an exact stoichiometry of the target products. Transparent phosphate–formate solutions of lithium and cobalt (nickel, respectively) were obtained by mixing the solutions of M(HCOO)₂·2H₂O (M = Co or Ni) and LiH₂PO₄ keeping a stoichiometric ratio M/Li = 1:1. The pH value of both solutions before mixing was adjusted to pH ≈ 3 with addition of a small quantity of HCOOH (1:1). In comparison with the iron and manganese salts, the solubility of Co(HCOO)₂ and Ni(HCOO)₂ in water is limited up to 2.7% at 25 °C. Therefore, in these cases the concentrations of freeze-dried solutions were varied between 0.05 and 0.10 M (with respect to the metal ions). The solutions thus prepared were frozen instantly with liquid nitrogen and dried in vacuo (20–30 mbar) for about 17 h at –20 °C with an Alpha-Christ Freeze Dryer. For the sake of simplicity, the precursors obtained from solutions with different concentrations will be further on denoted as PrCo-S005 and PrCo-S01, PrNi-S005 and PrNi-S01, i.e., obtained from 0.05 and 0.10 M solutions, respectively. After drying, the solid precursors were predecomposed at 350 and 400 °C for 3 h for cobalt and nickel precursors, respectively. The samples were further annealed at different temperatures from 350 to 750 °C for 10 h under static air atmosphere. The LiCoPO₄ and LiNiPO₄ samples obtained from the different precursors are denoted as LiCoPO₄-S005 and LiCoPO₄-S01, LiNiPO₄-S005 and LiNiPO₄-S01, respectively.

Methods for Sample Characterization: The metal content in starting M(HCOO)₂·2H₂O, the precursors, and LiMPO₄ (M = Co, Ni) samples was determined complexometrically. The lithium content was determined by atomic absorption analysis. Elemental analysis (C and H) was performed by using Elementar Analysensysteme GmbH (VarioEL analyzer). X-ray structural analysis was performed with a Bruker Advance 8 diffractometer with LynxEye detector by using Cu-K_α radiation. Step-scan recordings for structure refinement by the Rietveld method were carried out by using 0.02° 2θ steps of 10 s duration. The computer program FULLPROF was used in the calculations. The diffractometer point zero, the Lorentzian/Gaussian fraction of the pseudo-Voigt peak function, scale factor, the unit cell parameters (*a*, *b*, and *c*), the thermal factor for the 4a, 4c, and 8d positions and the line half-width parameters were determined. The crystallites size of LiMPO₄ was calculated by the Scherrer equation from the line width of the (200) reflection peak: $D_{200} = \lambda / [(\beta^2 - \beta_o^2)^{1/2} \cos \theta_{200}]$, where $\lambda(\text{Cu-K}\alpha) = 0.15418$ nm, β is the peak width at the half height corrected with instrumental broadening, and θ_{hkl} is the Bragg angle. The line width was determined by profile analysis using a WinPlotr program. The IR spectra were recorded with a Fourier transform Nicolet Avatar-320 instrument using KBr pellets (resolution < 2 cm⁻¹). The thermal analysis (simultaneously obtained DTA, TG, and DTG curves) of the precursors was carried out by a “Stanton Redcroft” apparatus

in the temperature range up to 650 °C, a heating rate of 5 °C/min, and sample mass of 10 mg. The morphology of the precursors and LiMPO₄ powders was observed by JEOL (JSM-5300 and JSM-5510) scanning electron microscopes.

Acknowledgments

Authors are grateful for the financial support of the National Science Fund of Bulgaria (Ch 1701/2007) and the National Centre for New Materials (DO-02-82/2008).

- [1] A. K. Padhi, K. S. Nanjundaswamy, J. B. Goodenough, *J. Electrochem. Soc.* **1997**, *144*, 1188–1194.
- [2] M. S. Whittingham, Y. Song, S. Lutta, P. Y. Zavalij, N. Chernova, *J. Mater. Chem.* **2005**, *15*, 3362–3379.
- [3] K. Amine, H. Yasuda, M. Yamachi, *Electrochem. Solid State Lett.* **2000**, *3*, 178–179.
- [4] J. Wolfenstine, J. Allen, *J. Power Sources* **2005**, *14*, 389–390.
- [5] W. F. Howard, R. M. Spotnitz, *J. Power Sources* **2007**, *165*, 887–891.
- [6] J. M. Loris, C. Pérez Vicente, J. L. Tirado, *Electrochem. Solid State Lett.* **2002**, *5*, A234–A237.
- [7] B. Jin, H.-B. Gu, K.-W. Kim, *J. Solid State Electrochem.* **2008**, *12*, 105–111.
- [8] N. N. Bramnik, K. Nikolowski, D. M. Trots, H. Ehrenberg, *Electrochem. Solid State Lett.* **2008**, *11*, A89–A93.
- [9] Gangulibabu, D. Bhuvaneshwari, N. Kalaiselvi, N. Jayaprakash, P. Periasamy, *J. Sol-Gel Sci. Technol.* **2009**, *49*, 137–144.
- [10] P. Deniard, A. M. Dulac, X. Rocquefelte, V. Grigorova, O. Lebacqz, A. Pasturel, S. Jobic, *J. Phys. Chem. Solids* **2004**, *65*, 229–233.
- [11] R. Vasanthi, D. Kalpana, N. G. Renganathan, *J. Solid State Electrochem.* **2008**, *12*, 961–969.
- [12] X. Huang, J. Ma, P. Wu, Y. Hu, J. Dai, Z. Zhu, H. Chen, H. Wang, *Mater. Lett.* **2005**, *59*, 578–582.
- [13] H. H. Li, J. Jin, J. P. Wei, Z. Zhou, J. Yan, *Electrochem. Commun.* **2009**, *11*, 95–98.
- [14] K. Rissouli, K. Benkhoulja, J. R. Ramos-Barrado, C. Julien, *Mater. Sci. Eng., B* **2003**, *98*, 185–189.
- [15] D. Shanmukaraj, R. Murugan, *Ionics* **2004**, *10*, 88–92.
- [16] V. Koleva, E. Zhecheva, R. Stoyanova, *J. Alloys Compd.* **2009**, *476*, 950–957.
- [17] E. Zhecheva, Ml. Mladenov, P. Zlatilova, V. Koleva, R. Stoyanova, *J. Phys. Chem. Solids* **2010**, *71*, 848–853.
- [18] V. Koleva, R. Stoyanova, E. Zhecheva, *Mater. Chem. Phys.* **2010**, *121*, 370–377.
- [19] V. Koleva, R. Stoyanova, E. Zhecheva, *Eur. J. Inorg. Chem.* **2010**, 127–131.
- [20] V. Koleva, H. Effenberger, *J. Solid State Chem.* **2007**, *180*, 956–967.
- [21] K. G. Kidd, H. H. Mantsch, *J. Mol. Spectrosc.* **1981**, *85*, 375–389.
- [22] K. Nakamoto, *Infrared and Raman Spectra of Inorganic and Coordination Compounds*, 4th ed., Wiley, New York, **1978**, p. 138.
- [23] A. Ait Salah, P. Jozwiak, K. Zaghib, J. Garbarczyk, F. Gendron, A. Manger, C. M. Julien, *Spectrochim. Acta* **2006**, *65A*, 1007–1113.
- [24] A. Novak, *Struct. Bonding (Berlin)* **1974**, *18*, 177–216.
- [25] J. Baran, T. Lis, M. Drozd, H. Ratajczak, *J. Mol. Struct.* **2000**, *516*, 185–202.
- [26] J. Xu, D. F. R. Gilson, I. S. Butler, *Spectrochim. Acta* **1998**, *A54*, 1869–1878.
- [27] K. Mouaïne, P. Becker, C. Carabatos-Nédelec, *Phys. Stat. Sol.* **1997**, *200*, 273–287.
- [28] P. Baraldi, *Spectrochim. Acta* **1979**, *35A*, 1003–1007.
- [29] V. Rosenband, A. Gany, *J. Mater. Proc. Technol.* **2004**, *153–154*, 1058–1061.
- [30] T. Meisel, Z. Halmos, K. Seybold, E. Pungor, *J. Thermal Anal.* **1975**, *7*, 73–80.
- [31] H. Ehrenberg, N. N. Bramnik, A. Senyshyn, H. Fuess, *Solid State Sci.* **2009**, *11*, 18–23.
- [32] M. Th. Paques-Ledent, P. Tarte, *Spectrochim. Acta* **1974**, *30A*, 673–689.
- [33] O. García-Moreno, M. Alvarez-Vega, F. García-Alvarado, J. García-Jaca, J. M. Gallardo-Amores, M. L. Sanjuán, U. Amador, *Chem. Mater.* **2001**, *13*, 1570–1576.

Received: April 12, 2010

Published Online: July 30, 2010